

ARTICLE

Received 6 Nov 2014 | Accepted 7 Jan 2015 | Published 2 Feb 2015

DOI: 10.1038/ncomms7235

OPEN

Targeting protein tyrosine phosphatase σ after myocardial infarction restores cardiac sympathetic innervation and prevents arrhythmias

R.T. Gardner¹, L. Wang², B.T. Lang³, J.M. Cregg³, C.L. Dunbar¹, W.R. Woodward⁴, J. Silver³,
C.M. Ripplinger² & B.A. Habecker¹

Millions of people suffer a myocardial infarction (MI) every year, and those who survive have increased risk of arrhythmias and sudden cardiac death. Recent clinical studies have identified sympathetic denervation as a predictor of increased arrhythmia susceptibility. Chondroitin sulfate proteoglycans present in the cardiac scar after MI prevent sympathetic reinnervation by binding the neuronal protein tyrosine phosphatase receptor σ (PTP σ). Here we show that the absence of PTP σ , or pharmacologic modulation of PTP σ by the novel intracellular sigma peptide (ISP) beginning 3 days after injury, restores sympathetic innervation to the scar and markedly reduces arrhythmia susceptibility. Using optical mapping we observe increased dispersion of action potential duration, supersensitivity to β -adrenergic receptor stimulation and Ca^{2+} mishandling following MI. Sympathetic reinnervation prevents these changes and renders hearts remarkably resistant to induced arrhythmias.

¹Department of Physiology and Pharmacology, Neuroscience Graduate Program, Oregon Health and Science University, Portland, Oregon 97239, USA.

⁴Department of Neurology, Oregon Health and Science University, Portland, Oregon 97239, USA. ²Department of Pharmacology, University of California, Davis, California 95616, USA. ³Department of Neurosciences, Case Western Reserve University, Cleveland, Ohio 44106, USA. Correspondence and requests for materials should be addressed to C.M.R. (email: criplinger@ucdavis.edu) or to B.A.H. (email: habecker@ohsu.edu).

Survivors of myocardial infarction (MI) remain at high risk for cardiac arrhythmias and sudden cardiac death¹. The infarct, or scar, generates an anatomical substrate that promotes re-entrant arrhythmias², and numerous studies indicate that altered sympathetic neurotransmission in the heart also plays a key role in the onset of post-infarct cardiac arrhythmias^{3–7}. Norepinephrine (NE) released from sympathetic nerves activates cardiac β -adrenergic receptors (β -AR) to modulate myocyte repolarization by altering transmembrane currents and Ca^{2+} homeostasis^{8–10}, and simply disrupting the normal organization of sympathetic innervation in an otherwise healthy heart is arrhythmogenic^{11,12}. Cardiac sympathetic function is altered in a region-specific manner following MI, and studies in animals and humans reveal denervation of the infarct and adjacent, viable (peri-infarct) myocardium^{13–17}. Three recent studies in patients with implanted cardioverter defibrillators (ICDs) suggest that the amount of sympathetic denervation after MI predicts the probability of serious ventricular arrhythmias^{18–20}. A detailed electrical mapping study in intact human hearts revealed that sympathetic denervation of the normal myocardium adjacent to the scar resulted in β -AR agonist supersensitivity and increased dispersion of repolarization that was arrhythmogenic²¹. These studies and others led to the model that inappropriate heterogeneity of sympathetic transmission across the left ventricle, and subsequent electrical remodelling of cardiac myocytes, is a major contributor to post-infarct arrhythmias in humans²².

The observation that the denervated myocardium adjacent to the infarct contributes to the generation of post-infarct arrhythmias²¹ was especially interesting to us because chondroitin sulfate proteoglycans (CSPGs) in the cardiac scar prevent reinnervation of the infarct and the adjacent myocardium by sympathetic axons²³. Although axons sprout and regenerate towards the scar²⁴, they are stopped near the outer edge of the infarct by CSPGs. In the absence of the CSPG receptor, protein tyrosine phosphatase receptor σ (PTP σ), sympathetic axons fully reinnervate undamaged peri-infarct tissue and hyperinnervate the infarct²³. Given the clinical significance of sympathetic denervation after MI^{18–21}, we were interested to determine whether restoring sympathetic innervation to the infarct and surrounding myocardium altered post-MI arrhythmia susceptibility.

We targeted PTP σ using both genetic and pharmacologic approaches in order to promote reinnervation of the infarct, and used electrocardiogram (ECG) telemetry to examine arrhythmia susceptibility. Transmembrane potential (V_m) and intracellular Ca^{2+} dynamics were assessed using *ex vivo* optical mapping in order to investigate the mechanisms underlying changes in arrhythmia susceptibility. MI caused dispersion of action potential duration (APD), supersensitivity to β -AR stimulation and Ca^{2+} mishandling. Restoring sympathetic innervation to the infarct and the surrounding tissue decreased arrhythmia susceptibility and normalized cardiac electrophysiology and Ca^{2+} dynamics, despite the presence of a scar.

Results

Targeting PTP σ restores innervation after MI and prevents arrhythmias. We previously observed²³ that CSPGs generated in the cardiac scar after ischaemia-reperfusion (I-R) prevented reinnervation of the infarct (Fig. 1a) despite high levels of nerve growth factor in the scar. The infarct becomes hyperinnervated in animals lacking the CSPG receptor PTP σ ²³ (Fig. 1b), confirming the crucial role for PTP σ in sympathetic denervation after MI. Since cardiac denervation is linked to risk for arrhythmia and cardiac arrest in human studies^{18–21}, we asked whether

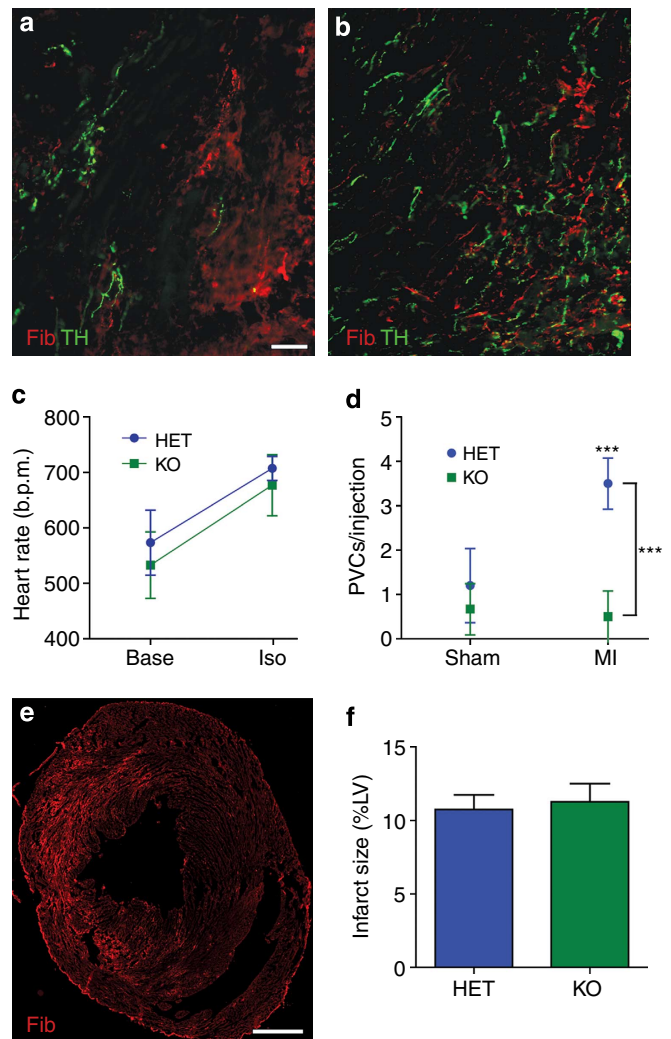


Figure 1 | Absence of PTP σ restores innervation to the infarcted

myocardium and prevents arrhythmias. Heart sections from HET (a) and KO (b) mice were stained for TH (green) to identify sympathetic nerve fibres and fibrinogen (red) to identify the infarct. Scale bar, 100 μm . (c) Heart rate was similar in both genotypes before (Base) and after (ISO) 10- μg ISO injection (mean \pm s.e.m., $n = 8$ per genotype). (d) ISO induced comparable levels of PVCs in conscious Sham HET and KO mice; however, ISO induced significantly more PVCs in infarcted HET mice compared with KO mice and to Sham HET mice (mean \pm s.e.m., $n = 4$ per group, *** $P < 0.001$ versus HET sham and KO MI; two-way ANOVA with Bonferroni post test). (e) Fibrinogen-stained section after MI showing a transmural infarct after a 35-min occlusion. Scale bar, 500 μm . (f) Quantification of infarct size in HET and KO hearts following 35 min of occlusion (mean \pm s.e.m., $n = 4$ per group; t -test, N.S. $P > 0.05$).

restoring sympathetic innervation to the infarct and surrounding myocardium affected arrhythmia susceptibility. Control mice heterozygous for PTP σ ($ptprs^{+/-}$; HET) and mice lacking PTP σ ($ptprs^{-/-}$; KO) were implanted with ECG telemetry transmitters and then subjected to sham or MI surgery. Ten days after surgery, the mice were injected with 10 μg of the beta agonist isoproterenol (ISO), which has also been used to induce arrhythmias in the clinical setting²⁵. ISO stimulated comparable increases in heart rate in all mice (Fig. 1c), but stimulated few premature ventricular complexes (PVCs) in sham mice of either genotype (Fig. 1d). In contrast, the arrhythmia response in post-MI animals differed on the basis of

the innervation status of the infarct. ISO stimulated a significant number of PVCs in HET mice with denervated infarcts (Fig. 1d); however, KO mice with innervated infarcts were resistant to ISO-induced arrhythmias, having the same number of PVCs as sham animals (Fig. 1d). Infarcts were generally transmural (Fig. 1e), and infarct size was the same in both genotypes (Fig. 1f) indicating that the difference in arrhythmia susceptibility could not be explained by scar size.

To confirm that reinnervation of the infarct and surrounding tissue decreased arrhythmia susceptibility, we sought to restore innervation in mice expressing normal levels of PTP σ . In order to promote regeneration of sympathetic axons through the CSPG-rich cardiac scar, we utilized ISP, developed by Lang and Silver²⁶ to target the intracellular dimerization domain of PTP σ . ISP restored growth of the central nervous system axons through CSPGs *in vitro*, and systemic injections of ISP enhanced axon sprouting through CSPGs after spinal cord injury *in vivo*²⁶. We asked whether targeting PTP σ with ISP could restore sympathetic axon regeneration into the cardiac scar. Wild-type (*ptprs*^{+/+}) mice were implanted with ECG telemetry transmitters, and a week later subjected to I-R surgery. Beginning 3 days after MI, when the infarct was fully denervated²⁴, mice were injected daily (intraperitoneal (IP)) with vehicle (5% dimethyl sulfoxide (DMSO)/Saline), ISP (10 μ mol; 44 μ g) or IMP (10 μ mol; 42 μ g) as a negative control. IMP targets the receptor PTP μ , which is not present in sympathetic neurons. Fourteen days after the MI surgery, the mice were treated with ISO to mimic circulating catecholamines and provoke arrhythmias, and hearts were collected for analysis of sympathetic innervation. Animals treated with either vehicle or IMP had denervated infarcts (Fig. 2a,b,d), whereas animals treated with ISP had normal levels of sympathetic innervation throughout the left ventricle, including the infarct (Fig. 2c,d). Thus, daily ISP injections beginning 3 days after the injury, when denervation was well established, allowed robust regeneration of sympathetic axons into the CSPG-laden cardiac scar.

Several studies indicate that newly regenerating sympathetic axons in the damaged heart have low levels of NE^{27,28}, likely because of local depletion of Tyrosine Hydroxylase (TH) by inflammatory cytokines²⁹. The cardiac scar in the mouse heart is mature by 10–12 days after reperfusion, and acute inflammation has resolved³⁰. Therefore, we quantified NE levels in the infarct and peri-infarct myocardium 14 days after surgery to determine whether the axons that had reinnervated the infarct and surrounding myocardium had normal NE levels. NE content was low in the denervated infarct of vehicle-treated animals, but was normal in the innervated infarct of ISP-treated animals (Fig. 2e). NE content in the undamaged portion of the left ventricle was similar in both treatment groups (Fig. 2e), consistent with identical innervation densities (Fig. 2d). Likewise, NE content in the undamaged right ventricle was similar in both groups (Veh versus ISP; 5.50 ± 0.70 versus 6.38 ± 0.81 pmol mg⁻¹; $P=0.43$). These data indicate that restoring innervation to the infarct with ISP normalizes NE levels across the left ventricle by 2 weeks after MI.

Since regional sympathetic denervation is thought to be an important source of post-MI arrhythmia susceptibility in humans, we quantified ISO-induced arrhythmia 14 days after MI in mice treated with vehicle, IMP or ISP. ISO triggered significantly fewer PVCs in ISP-treated mice, which had innervated infarcts and normal NE content, than in the vehicle or IMP-treated groups, which had denervated infarcts and low NE content (Fig. 2f). These data suggest that restoring sympathetic transmission throughout the infarcted left ventricle, even days after denervation is established, is sufficient to decrease arrhythmia susceptibility.

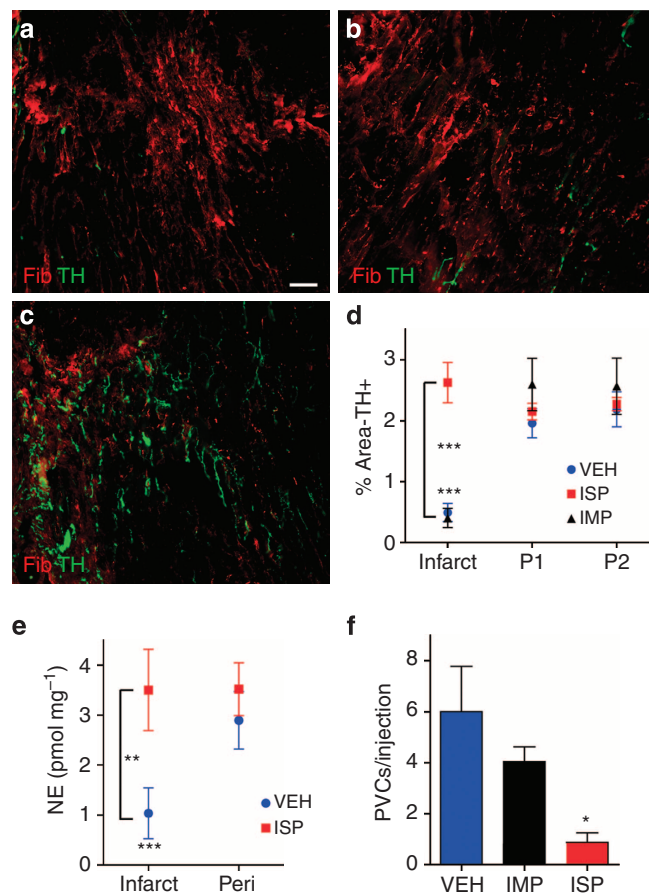


Figure 2 | ISP promotes sympathetic reinnervation of the infarct and decreases arrhythmias.

(a–c) Representative images of infarcted LV from mice treated with vehicle (a), IMP (b) or ISP (c) 14 days after MI. Sections were stained for TH (green) to identify sympathetic nerve fibres and fibrinogen (red) to identify the infarct. ISP treatment resulted in extensive sympathetic reinnervation of the infarct. Scale bar, 100 μ m. (d) Quantification of TH+ fibre density within the infarct, the area immediately adjacent to the infarct (P1) and distal peri-infarct myocardium (P2; 540 μ m from infarct) 14 day post-MI (mean \pm s.e.m., $n=5$ per group; $***P<0.001$ by two-way ANOVA with Bonerroni post test). (e) NE content in the infarct and peri-infarct LV (P1 and P2 combined; mean \pm s.e.m.; $n=5$; $**P<0.01$, $***P<0.001$ by two-way ANOVA with Bonerroni post test). (f) ISO induced PVCs in conscious mice 14 days after MI (mean \pm s.e.m., $n=4-5$; $*P<0.05$ versus vehicle and IMP by ANOVA with Tukey post test). Vehicle and IMP groups are not significantly different.

Reinnervation limits dispersion of APD and β -AR supersensitivity.

Activation of cardiac β receptors decreases myocyte APD by changing ion channel activity and Ca²⁺ handling to allow for adaptation to fast heart rates^{8–10}. In order to assess directly the impact of infarct reinnervation on cardiac electrophysiology, we used optical mapping to simultaneously image intracellular Ca²⁺ and V_m in Langendorff-perfused isolated hearts. PTP KO mice were used to examine the effect of reinnervation on cardiac electrophysiology, with *ptprs*^{+/-} (HET) mice serving as denervated controls.

In order to compare baseline electrical properties, a pacing electrode was positioned on the base of the LV epicardium (Fig. 3a), and APD at 90% repolarization (APD₉₀) was assessed at a pacing interval of 150 ms (400 b.p.m. heart rate). Figure 3b (top) shows a representative example of action potential propagation across a heart from each group: HET Sham, KO Sham, HET MI and KO MI. Figure 3b (bottom) shows a representative map of

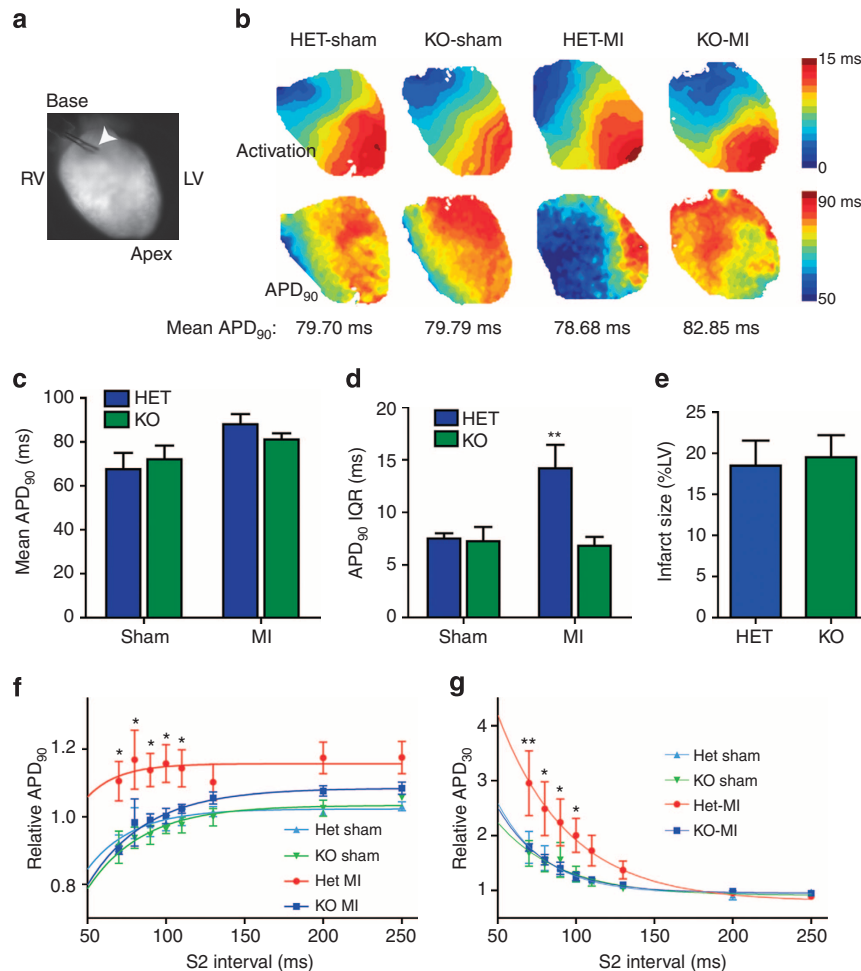


Figure 3 | Sympathetic innervation of the infarct reduces dispersion of APD. (a) Image of a heart prepared for mapping. All maps are represented in this same orientation. White arrow head indicates stimulating electrodes; infarct region is in the apical LV. (b) Activation maps of transmembrane potential (V_m) show propagation of a stimulus depolarization event spreading from the base to apex of the heart (top), and representative maps of APD₉₀ (bottom). (c) The mean APD₉₀ is similar in all groups (mean \pm s.e.m.; $n = 4-5$ hearts per group). (d) IQR of APD₉₀, a measure of APD dispersion (mean \pm s.e.m.; $n = 4-5$, $**P < 0.01$ by two-way ANOVA with Bonferroni post test). Hearts with denervated infarcts (HET MI) have increased APD dispersion compared with sham hearts, while hearts with innervated infarcts (KO MI) do not. (e) Infarct size in HET and KO hearts following 45 min of occlusion (mean \pm s.e.m., $n = 5$ per group). Restitution curves of (f) late repolarization (APD₉₀) and (g) early repolarization (APD₃₀; mean \pm s.e.m., $n = 4-5$; $**P < 0.01$, $*P < 0.05$ versus all other groups by two-way ANOVA with Bonferroni post test).

APD₉₀ throughout each heart. Quantification of the mean APD₉₀ revealed that it was similar across all four groups (Fig. 3c). However, it is clear that the denervated HET MI heart exhibits greater extremes of APD₉₀ than the other hearts. The inter-quartile range (IQR) is a measure of APD₉₀ variability, or dispersion, across an individual heart. IQR was significantly higher in denervated HET MI hearts compared with all other groups (Fig. 3d), consistent with increased dispersion of APD after MI in human studies²¹. Analysis of regional APD revealed a significant difference between the denervated infarct and normal myocardium (Supplementary Fig. 1). Surprisingly, sympathetic reinnervation of the infarct in KO hearts prevented an increase in APD dispersion following MI (Fig. 3d), even though the infarct size in the KO MI group was identical to that in the HET MI group (Fig. 3e).

Cycle length-dependent changes in APD (known as APD restitution) have also been implicated in arrhythmia generation³¹; therefore, we generated APD restitution curves using the pacing interval of 150 ms (S1) followed by a single extrastimulus (S2), with consecutively shorter S2 intervals. As expected, conduction velocity (Supplementary Fig. 2) and APD₉₀ decreased with

shorter S2 intervals in all hearts (Fig. 3f), while APD₃₀ increased (Fig. 3g), consistent with previous studies of these properties in the mouse heart³². Interestingly, the HET MI hearts exhibited limited APD₉₀ shortening compared with the other groups (Fig. 3f), and early repolarization (APD₃₀) was blunted in those hearts at shorter S2 intervals (Fig. 3g). The increased APD₃₀ observed in HET MI hearts is consistent with the reduction in transient outward K⁺ current (I_{to}) seen after MI or sympathetic denervation^{33,34}. However, KO MI hearts with sympathetic reinnervation exhibited APD restitution properties that were indistinguishable from sham hearts.

Sudden cardiac death is most common in the morning³⁵, when circulating catecholamines (NE and epinephrine) are rising rapidly³⁶. Given the protective role of beta blockers in humans, and the observation that PVCs induced by the beta agonist ISO are a good marker of arrhythmia propensity in humans²⁵, we examined the role of β -AR activation in arrhythmia generation in our infarcted mouse hearts. We treated hearts with tyramine to induce the release of endogenous NE from sympathetic axons within the heart, and with ISO to mimic circulating catecholamines. Release of endogenous NE with tyramine

resulted in similar APD shortening across all groups (% change: HET Sham -0.5 ± 0.6 , HET MI -0.8 ± 0.6 , KO Sham -0.2 ± 0.2 , KO MI -2.1 ± 0.6 ; $n = 3-5$, mean \pm s.e.m.). In contrast, treatment with ISO, which mimics the effect of circulating catecholamines *in vivo*, stimulated a significantly greater shortening of APD₉₀ in denervated HET MI hearts compared with all other groups (Fig. 4a,b). This denervation-induced β -AR supersensitivity is consistent with recent human data²¹. Consistent with the baseline data, APD₉₀ dispersion (IQR) remained elevated in the HET MI hearts following ISO treatment (Fig. 4c).

Sympathetic reinnervation prevents Ca²⁺ mishandling and PVCs. In order to identify additional mechanisms underlying changes in cardiac electrophysiology, we examined intracellular Ca²⁺ handling at various pacing frequencies and after ISO treatment. Disrupted Ca²⁺ homeostasis can result in beat-to-beat fluctuations between large and small intracellular calcium transients (Ca_T) called alternans, which is a sensitive noninvasive marker for the risk of sudden cardiac death in humans³⁷. Intracellular Ca²⁺ handling appeared normal in sham hearts of both genotypes when paced with a 100-ms pulse interval (600 b.p.m. heart rate; Fig. 5). However, HET hearts with denervated infarcts (HET MI) exhibited significant intracellular Ca²⁺ alternans at the same pacing frequency (Fig. 5). Interestingly, KO hearts with innervated infarcts (KO MI) did not exhibit intracellular Ca²⁺ alternans (Fig. 5), suggesting that restoring sympathetic innervation to the infarct and surrounding tissue protects intracellular Ca²⁺ homeostasis. Denervated HET MI hearts also exhibited significant APD alternans (Fig. 5c), while innervated KO MI hearts did not, despite identical infarct size.

The notion that sympathetic reinnervation of the peri-infarct border and scar protects intracellular Ca²⁺ handling was

confirmed by analysing intracellular Ca²⁺ dynamics after ISO administration. Under baseline conditions, normal excitation-contraction coupling occurred, in which membrane depolarization (V_m; black) preceded the Ca_T upstroke (red) in hearts from both genotypes and surgical groups (Fig. 6a, inset). In sham hearts treated with ISO, depolarization continues to precede the Ca_T (Supplementary Fig. 3). However, in the infarcted hearts, the response to ISO differed depending on the innervation status. Infarcted hearts with sympathetic innervation restored throughout the entire left ventricle (KO MI) continued to exhibit normal Ca²⁺ handling after ISO treatment (Fig. 6a,b), while hearts with sympathetic denervation (HET MI) exhibited pathological increases in diastolic intracellular [Ca²⁺] that preceded membrane depolarization (Fig. 6a,b). This Ca²⁺ elevation was prevented by addition of the β -AR blocker propranolol (Fig. 6a,b).

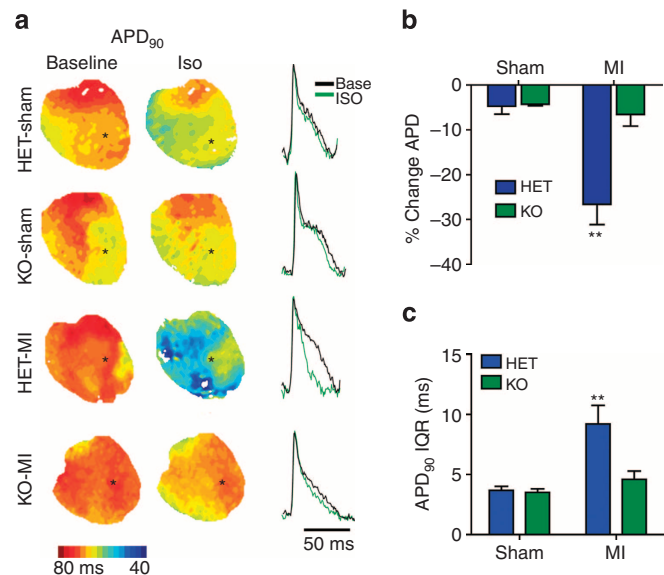


Figure 4 | Sympathetic innervation of the infarct prevents β -AR supersensitivity. (a) APD₉₀ maps before (Baseline) and after 1- μ M ISO (100-ms pacing interval or 600 b.p.m. heart rate for each condition), and representative traces of optical action potentials from sites marked with *. Scale bar, 50 ms. (b) Percent change in APD₉₀ following ISO treatment (mean \pm s.e.m.; $n = 4-5$ hearts per group; ** $P < 0.01$ by two-way ANOVA with Bonferroni post test). (c) IQR of APD₉₀ following ISO treatment (mean \pm s.e.m.; $n = 4-5$ hearts; ** $P < 0.01$ by two-way ANOVA with Bonferroni post test).

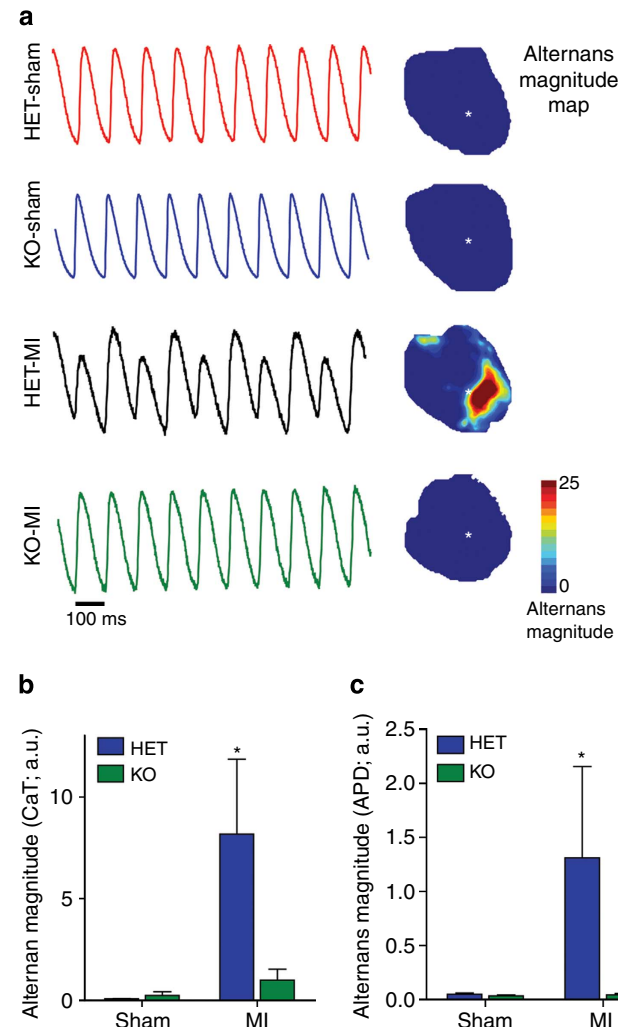


Figure 5 | Sympathetic innervation of the infarct prevents post-MI Ca²⁺ mishandling. (a) Representative optical Ca²⁺ transients and alternans maps from the sites on sham and post-MI hearts marked (*) paced with a 100-ms pacing interval (600 b.p.m. heart rate). Scale bar, 100 ms. Denervated hearts (HET MI) exhibit Ca²⁺ alternans, while sham hearts and infarcted hearts with sympathetic innervation of the scar (KO MI) do not. (b) Intracellular Ca²⁺ alternans magnitude was quantified by spectral analysis (mean \pm s.e.m.; $n = 4-5$ hearts; * $P < 0.05$ versus other groups by two-way ANOVA with Bonferroni post test). (c) APD alternans magnitude was quantified by spectral analysis (mean \pm s.e.m.; * $P < 0.05$ versus sham using Kruskal-Wallis test for non-Gaussian distribution).

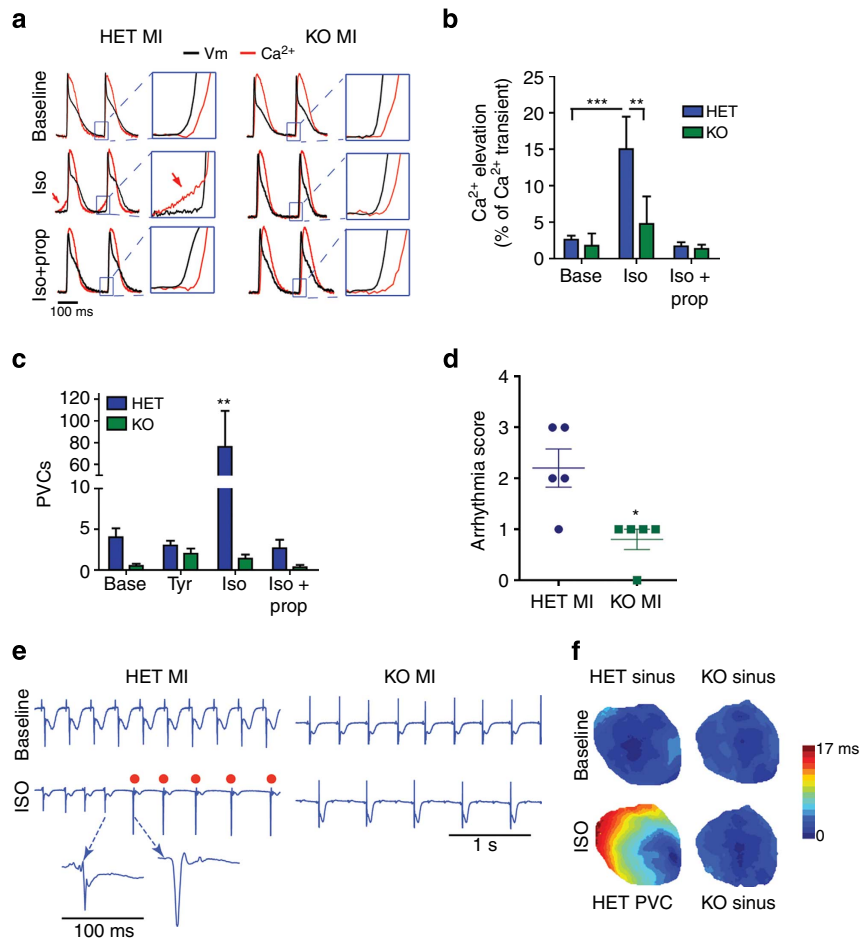


Figure 6 | Reinnervation of the infarct prevents Ca^{2+} mishandling and ventricular arrhythmias. (a) Representative optical V_m and Ca^{2+} transients in HET and KO hearts at baseline (Base), with ISO, and with both ISO and propranolol (Iso + Prop). Red arrows indicate Ca^{2+} elevation before V_m depolarization. Scale bar, 100 ms. Insets show an expanded timescale of V_m and CaT upstrokes. (b) Quantification of CaT elevation that precedes depolarization averaged across the entire surface of the heart (mean \pm s.e.m.; $n = 4-5$ hearts; $**P < 0.01$, $***P < 0.001$ by two-way ANOVA with Bonferroni post test). (c) Incidence of PVCs during baseline stimulation and treatment with tyramine (Tyr), ISO (Iso) and ISO plus propranolol (Iso + Prop; mean \pm s.e.m.; $n = 4-5$ hearts; $**P < 0.01$ versus all other groups by two-way ANOVA with Bonferroni post test). (d) Arrhythmia severity of HET MI and KO MI hearts during ISO treatment. Individual hearts are scored on the basis of the most severe arrhythmia observed (mean \pm s.e.m.; $n = 4-5$ hearts; $*P < 0.05$ by t -test). (e) Example Lead I ECGs from *in vitro* Langendorff-perfused hearts during baseline and with ISO. Owing to ISO-induced acceleration of the sinus rate, hearts in both groups exhibited atrioventricular (A-V) block (see P-wave dissociation and 3:1 A-V block in ISO traces); however, PVCs were significantly more frequent in HET MI hearts (red dots). PVCs were readily identified by a large and wide QRS complex compared with the normal (sinus or nodal) QRS complex (inset). (f) Representative activation maps in HET MI and KO MI hearts depicting rapid activation during sinus rhythm (Base line) in both hearts and with ISO treatment (Iso) in the KO MI heart. Iso treatment in the denervated (HET MI) heart produced PVCs with slowly propagating activation arising from the infarct region.

We previously showed that strong localized β -AR stimulation can trigger Ca^{2+} release independent of membrane depolarization that is sufficient to cause PVCs³⁸. Therefore, we asked whether ISO-stimulated Ca^{2+} mishandling led to the production of PVCs after MI. Quantification of *in vitro* arrhythmia severity in HET and KO MI hearts confirmed the striking difference in arrhythmia susceptibility observed during the *in vivo* ECG telemetry studies. Arrhythmia severity was scored on the basis of the most severe arrhythmia observed in each heart over a 20-min continuous ECG recording (0 = no PVCs, 1 = single PVCs, 2 = bigeminy or salvos and 3 = ventricular tachycardia)³⁹. Sham animals of both genotypes exhibited only single PVCs, and ISO stimulated a similar number in both genotypes (HET versus KO; Base: 1.00 ± 0.71 versus 1.33 ± 0.88 and Iso: 1.75 ± 0.48 versus 1.33 ± 0.33). ISO triggered significantly more arrhythmias in HET MI hearts with denervated infarct/peri-infarct tissue compared with all other

groups (Fig. 6c,e), and it stimulated arrhythmias of greater severity in those hearts, including ventricular tachycardia (Fig. 6d). In contrast, KO MI hearts with innervated infarct/peri-infarct tissue exhibited only individual PVCs and the number of PVCs was similar to that seen in the sham groups (Fig. 6c), even though infarct size was comparable to HET MI hearts. As expected, administration of propranolol prevented ISO-induced arrhythmias in HET MI hearts, confirming the role of β -AR (Fig. 6c). Importantly, Ca^{2+} mapping revealed that the Ca^{2+} elevation induced by ISO was associated with PVCs arising from the infarct region (Fig. 6f). All PVCs that were captured during a mapping procedure arose from the region of the infarct, suggesting that denervation-induced β -AR supersensitivity leads to diastolic Ca^{2+} elevation near the infarct that is sufficient to trigger PVCs. Restoration of sympathetic innervation to the infarct and surrounding tissue normalizes Ca^{2+} handling and makes hearts resistant to ISO-induced arrhythmias.

Discussion

The observation that local sympathetic denervation in the post-MI heart leads to high arrhythmia risk seems to contradict the many clinical studies showing that blocking sympathetic transmission in the heart, either with beta blockers or with surgical ganglionectomy, prolongs life after MI^{3,6,7,40,41}. However, a consensus has developed that inappropriate heterogeneity of sympathetic transmission in the heart, and subsequent electrical remodelling of cardiac myocytes, is arrhythmogenic²². This heterogeneity can be caused by the loss of sympathetic transmission in a portion of the heart^{18–21}, or it can be caused by regional nerve sprouting and hyperinnervation^{42–46}. In this context, surgical denervation and administration of beta blockers can be seen as methods for ‘evening out’ sympathetic transmission across the heart by decreasing it everywhere. Our data fully support the model that heterogeneity of sympathetic transmission after MI is pathological; however, our approach to correct that problem was to restore sympathetic transmission throughout the left ventricle by targeting PTP σ . It is especially notable that we were able to restore innervation using a pharmacologic intervention that was initiated several days after injury when the infarct and peri-infarct myocardium was already denervated. Daily injections with ISP were sufficient to restore functional sympathetic innervation, and reinnervation rendered hearts surprisingly resistant to arrhythmias. Indeed, infarcted hearts with restored sympathetic innervation were electrically indistinguishable from sham hearts, despite the presence of a scar.

This work has implications for patients who survive a MI, and remain at risk for severe cardiac arrhythmias and sudden cardiac death¹. Those patients who have a left ventricular (LV) ejection fraction $\leq 35\%$ often receive prophylactic implantation of an ICD⁴⁷; however, low ejection fraction has not proven to be a good predictor of those truly in need of ICDs⁴⁸. Substantial effort has gone into identifying parameters that can predict those patients most likely to benefit from ICDs, and three recent trials found that sympathetic denervation within the heart after MI predicted the incidence of sudden cardiac arrest and arrhythmia independent of infarct size and LV ejection fraction^{18–20}. Our study provides a mechanistic link between post-infarct denervation and altered beta receptor responsiveness, calcium handling and arrhythmia susceptibility.

There are limitations, however, to the mouse model for studies of cardiac rhythm disturbances, as the repolarizing currents in the rodent heart are different from those in larger species^{32,49}. In addition, the scar formed in the mouse heart contains less collagen than the scar in larger animals³⁰, and that might have an impact on arrhythmia susceptibility. Other limitations of our experimental model are not unique to the mouse. For example, we used ISO or electrical stimulation protocols to trigger arrhythmias because spontaneously occurring arrhythmias were relatively rare events in our mice. However, arrhythmias are rare even in patients with significant LV systolic dysfunction following MI, exemplified by the fact that it takes many years to demonstrate benefit from an ICD in such populations⁴⁸. Thus, interventions including exercise stress testing⁵⁰ or ISO²⁵ are used by clinicians to evoke arrhythmias in the clinic, and PVCs triggered by these methods are indicative of arrhythmia propensity in humans. Therefore, our data suggest a potential site for therapeutic intervention, but future studies are necessary to test the anti-arrhythmic efficacy of ISP in larger animal models.

These data provide an important validation of the hypothesis that targeting PTP σ can promote nerve regeneration through CSPG-containing scars *in vivo*, and suggest that reversing infarct-induced sympathetic denervation is protective for the heart. MI is an ideal target for PTP σ -based therapeutics because the cardiac scar contains high levels of nerve growth factor and simply

removing PTP σ is sufficient to promote reinnervation of the infarct²³. However, these data also have important implications for the treatment of spinal cord injury and other peripheral nerve injuries where CSPG-PTP σ interactions prevent nerve regeneration. Systemic injection of the peptide ISP was effective in restoring axon regeneration through CSPGs in the cardiac scar and decreasing arrhythmia risk. This raises the possibility that targeting PTP σ using a simple systemically deliverable peptide in patients who have survived a MI might promote reinnervation of otherwise denervated cardiac tissue, and that normalizing the innervation might decrease arrhythmia risk.

Methods

Animals. PTP σ (ptprs) transgenic mice (BalbC) were supplied by Michel Tremblay (McGill University)⁵¹ and were bred as heterozygotes²³. Age- and gender-matched mice that were 12–18 weeks old were used for all experiments. ptp σ + / – (HET) littermates were used as controls for ptp σ – / – (KO) studies. Some ptp σ + / + mice were given daily IP injections of vehicle (5% DMSO/Saline), IMP (Intracellular Mu Peptide; 10 μ mol) or ISP (10 μ mol) beginning 3 days after I–R. All mice were kept on a 12:12 h light–dark cycle with ad libitum access to food and water. All procedures were approved by the OHSU and the University of California–Davis Institutional Animal Care and Use Committee and comply with the Guide for the Care and Use of Laboratory Animals published by the National Academies Press (8th edition).

Surgery. (1) *Myocardial I–R*: Anaesthesia was induced with 4% isoflurane and maintained with 2% isoflurane. The left anterior descending coronary artery was reversibly ligated for 30 min (telemetry studies) or 45 min (*ex vivo* mapping) and then reperused by release of the ligature^{23,24}. Occlusion was confirmed by sustained S–T wave elevation and regional cyanosis. Reperfusion was confirmed by the return of colour to the ventricle distal to the ligation and reperfusion arrhythmia. Core body temperature was monitored by a rectal probe and maintained at 37 °C, and a two-lead ECG was monitored. (2) *Sham surgery*: Sham animals underwent the procedure described above, except for the left anterior descending coronary artery ligation.

In vivo telemetry. ECGs were obtained from conscious adult mice using ETA-F10 (Data Sciences International) telemetry implants, and were analysed with the Dataquest ART software (Data Sciences International). Mice were anaesthetized with 4% and maintained on 2% inhaled isoflurane. A transmitter was implanted subcutaneously in a lead II configuration, with the negative lead placed in the right pectoral muscle and the positive lead to the left of the xyphoid process. Devices were implanted at least 5 days before I–R or sham surgery¹².

ECG recordings were obtained 10 (PTP σ transgenic studies) or 14 (ISP studies) days after sham or MI surgery. ECGs were analysed beginning 60 min before IP injection of a relatively low dose of the β -AR agonist ISO (10 μ g or ~ 0.5 mg kg^{–1})^{52,53} as a baseline, and then for 60 min after injection to identify ISO-induced arrhythmias. PVCs were defined as a single premature QRS complex in the absence of a P-wave. Heart rate was analysed to confirm that the SA node response to ISO was similar between groups.

Immunohistochemistry. Hearts were fixed for 1 h in 4% paraformaldehyde, rinsed in PBS, cryoprotected in 30% sucrose overnight and frozen in mounting medium for sectioning. Transverse 10- μ m sections were cut on a cryostat and thaw-mounted on charged slides. To reduce fixative-induced autofluorescence, sections were rinsed in 10 mg ml^{–1} sodium borohydride for 3 \times 10 min and then rinsed in PBS for 3 \times 10 min. The sections were then blocked in 3% BSA/0.3% Triton X-100 in PBS for 1 h. The slides were then incubated with rabbit anti-TH (1:1,000, Millipore/Chemicon) and sheep anti-fibrinogen (1:500, AbD Serotec) antibodies overnight at 4 °C, rinsed for 3 \times 10 min in PBS and incubated for 1.5 h with the AlexaFluor 488-conjugated rabbit IgG-specific antibody (1:1,000; Invitrogen) and AlexaFluor 568-conjugated sheep IgG-specific antibody (1:1,000). Sections were rinsed for 3 \times 10 min in PBS, incubated for 30 min in 10 mM CuSO₄ in 50 mM ammonium acetate to reduce background signal further, rinsed for 3 \times 10 min in PBS, coverslipped in a 1:1 PBS:glycerol solution and visualized using fluorescence microscopy.

Imaging and threshold analysis. TH staining was quantified to assess sympathetic innervation density. Images were taken of the infarct, proximal and distal peri-infarct zone of each section, and three sections obtained from a similar level of the base-to-apex axis were quantified in each heart using threshold discrimination analysis. Black and white photos were opened in ImageJ and the brightness/contrast tool was used to adjust each image so that the minimum was set at the left side of the histogram. The threshold tool was then used to identify nerve fibres. The automated function set a beginning threshold level; however, this did not reliably include all sympathetic fibres while excluding all non-neuronal tissues. The

threshold was then manually adjusted to ensure that only specific TH staining was identified. The ventricle has two layers of muscle set at different angles; therefore, each section included some nerve fibres cut longitudinally along the plane of the section and other fibres cut in cross-section and appearing as small round dots. Thus, specific criteria for size and shape were not used in our analysis. Innervation density was expressed as the percent of area that was above the threshold (TH + fibres). Each image was quantified by two independent observers.

Infarct size. Infarcts were identified with fibrinogen staining and infarct size was quantified using eight 10- μm sections, $\sim 200\ \mu\text{m}$ apart obtained from matched levels from each heart. Images were taken of the entire section, and the LV and infarct areas were measured by outlining the respective regions using the freehand selection tool in ImageJ. Infarct size was then calculated as a percentage of the LV area [(infarct area/LV area) $\times 100$]. Sections were obtained from the upper, middle and lower regions of the infarct in each heart.

NE content. NE levels in heart tissue were measured using HPLC with electrochemical detection. Frozen, pulverized tissue was weighed, and then homogenized in 0.2 M perchloric acid and 0.5 μM dihydroxybenzylamine (DHBA). The tissue was refrigerated for 1 h and centrifuged at 14,000 r.p.m. for 4 min. Supernatant was adsorbed on alumina, followed by 15 min of tumbling. The alumina was washed twice with 1.0 ml of H_2O with centrifugations in between. The NE was desorbed from the alumina with 150 μl of 0.1 M perchloric acid. Fifty-microlitre aliquots were fractionated by reversed-phase HPLC (C18; 5 μm particle size, Rainin) using a mobile phase containing 75 mM sodium phosphate (pH 3.0), 360 mg l^{-1} of sodium octane sulfonate, 100 $\mu\text{l l}^{-1}$ triethylamine and 3.0% acetonitrile. A coulometric detector (Coulchem, ESA) was used to detect and quantify NE and DHBA. NE standards (0.5 μM) were processed in parallel with tissue samples and interspersed throughout the HPLC run. Retention time for NE was 5.0 min and for DHBA was 8.5 min.

Langendorff perfusion and dual optical mapping of V_m and Ca^{2+} . Mice were anaesthetized with pentobarbital sodium (150 mg kg^{-1} , IP) containing 120 IU of heparin. Following a midsternal incision, hearts were rapidly excised and Langendorff-perfused at 37 $^\circ\text{C}$ with oxygenated (95% O_2 and 5% CO_2) modified Tyrode's solution of the following composition (in mmol l^{-1}): NaCl 128.2, CaCl_2 1.3, KCl 4.7, MgCl_2 1.05, NaH_2PO_4 1.19, NaHCO_3 20 and glucose 11.1 (pH 7.4). Flow rate (1.5–3.5 ml min^{-1}) was adjusted to maintain a perfusion pressure of 60–80 mm Hg. One leaflet of the mitral valve was carefully damaged with sharp forceps inserted through the pulmonary vein to prevent solution congestion in the LV cavity after suppression of ventricular contraction. Two Ag/AgCl disc electrodes were positioned in the bath to record an ECG analogous to a lead I configuration. ECG was continuously recorded throughout the duration of the experiment. A bipolar electrode was positioned on the base of the LV epicardium for pacing, which was performed at a basic cycle length of 150 ms using a 2-ms pulse width at twice the diastolic threshold.

Hearts were loaded with the fluorescent intracellular Ca^{2+} indicator Rhod-2 AM (Molecular Probes, Eugene, OR; 50 μl of 1 mg ml^{-1} in DMSO containing 10% pluronic acid) and were subsequently stained with the voltage-sensitive dye RH237 (Molecular Probes; 10 μl of 1 mg ml^{-1} in DMSO). Blebbistatin (Tocris Bioscience, Ellisville, MO; 10–20 μM) was added to the perfusate to eliminate motion artifact during optical recordings. The anterior epicardial surface was excited using LED light sources centred at 530 nm and bandpass-filtered from 511 to 551 nm (LEX-2, SciMedia, Costa Mesa, CA) and focused directly on the surface of the preparation. The emitted fluorescence was collected through a 50-mm objective (Nikon, Japan) and split with a dichroic mirror at 630 nm (Omega, Brattleboro, VT). The longer wavelength moiety, containing the V_m signal, was longpass-filtered at 700 nm and the shorter wavelength moiety, containing the Ca^{2+} signal, was bandpass-filtered between 574 and 606 nm. The emitted fluorescence signals were recorded using two CMOS cameras (MiCam Ultima-L, SciMedia) with a sampling rate of 1 kHz and 100 \times 100 pixels with a 10 \times 10 mm field of view³⁸.

Mapping experimental protocol. Following dye loading, baseline electrophysiological parameters were recorded during normal sinus rhythm as well as LV epicardial pacing at intervals of 150 and 100 ms. Hearts were subjected to tyramine infusion (20 μM) followed by a washout period. Hearts were then subjected to acute β -AR stimulation with ISO (1 μM). Optical recordings were taken every 5 min following treatment, and ECG was continuously recorded. Following 15 min of ISO treatment, the β -AR blocker propranolol (10 μM) was added to the perfusate. Optical recordings were repeated every 5 min for 15 min.

Optical mapping data analysis. Optical mapping data analysis was performed using two commercially available analysis programmes (BV_Analyze, Brainvision, Tokyo, Japan and Optiq, Cairn, UK). V_m and Ca^{2+} data sets were spatially aligned and processed with a Gaussian spatial filter (radius 3 pixels). For both action potentials and Ca_T , activation time was determined as the time at 50% of the maximal amplitude. For action potentials, repolarization time at 30 and 90% return to baseline were used to calculate APD (APD₃₀ and APD₉₀). Relative APD₃₀ and

APD₉₀ used in restitution curves were calculated as a ratio of S2 APD/S1 APD. Conduction velocity was calculated along a vector from the base to apex using a polynomial fitting algorithm previously described in ref. 54. Separate measurements of longitudinal and transverse conduction velocity were not determined because of the basal pacing location and disruption of fibre orientation in the infarct region. Diastolic Ca^{2+} elevation was measured as the percentage of diastolic Ca^{2+} increase relative to the following Ca_T amplitude at baseline and 15 min post treatment. The average diastolic Ca^{2+} elevation was calculated for each heart by averaging all Ca^{2+} signals from the entire anterior surface of the heart within the optical mapping field of view. PVC incidence was determined from the continuous ECG recording as the number of PVCs that occurred during a 20-min period of baseline activity (before initiation of treatment) and during the 20 min of treatment. Arrhythmia severity was scored on the basis of the most severe arrhythmia observed in each heart over a 20-min continuous ECG recording (0 = no PVCs, 1 = single PVCs, 2 = bigeminy or salvos and 3 = ventricular tachycardia)³⁹.

The spectral method, which has been used clinically for detecting micro-volt T-wave alternans⁵⁵, was used to detect the presence of Ca_T alternans and APD alternans⁵⁶. The spectral method was chosen because of its high sensitivity and relative immunity to noise. This approach allowed us to determine whether an area within the mapping field of view was experiencing significant APD or Ca_T alternans (greater than the background noise levels) as well as the spatial extent of significant alternans. A spectral magnitude of ≥ 2 was used as the minimum threshold for significant APD or Ca_T alternans, corresponding to a beat-to-beat change in APD₉₀ ≥ 5 ms or beat-to-beat change in Ca_T amplitude $\geq 5\%$, respectively⁵⁷.

Statistics. Student's *t*-tests were used to compare two groups. Data sets that included more than two groups were analysed by one-way analysis of variance (ANOVA) using the Tukey *post hoc* test to compare all conditions. For experiments comparing different surgical groups and genotypes a two-way ANOVA was carried out using the Bonferroni *post hoc* test. All statistical analyses were carried out using Prism 5.0.

References

- Solomon, S. D. *et al.* Sudden death in patients with myocardial infarction and left ventricular dysfunction, heart failure, or both. *N. Engl. J. Med.* **352**, 2581–2588 (2005).
- Jalife, J. Ventricular fibrillation: mechanisms of initiation and maintenance. *Annu. Rev. Physiol.* **62**, 25–50 (2000).
- Nademanee, K., Taylor, R., Bailey, W. E., Rieders, D. E. & Kosar, E. M. Treating electrical storm: sympathetic blockade versus advanced cardiac life support-guided therapy. *Circulation* **102**, 742–747 (2000).
- Basu, S. *et al.* Beneficial effects of intravenous and oral carvedilol treatment in acute myocardial infarction. A placebo-controlled, randomized trial. *Circulation* **96**, 183–191 (1997).
- Billman, G. E., Castillo, L. C., Hensley, J., Hohl, C. M. & Altschuld, R. A. Beta2-adrenergic receptor antagonists protect against ventricular fibrillation: in vivo and in vitro evidence for enhanced sensitivity to beta2-adrenergic stimulation in animals susceptible to sudden death. *Circulation* **96**, 1914–1922 (1997).
- Exner, D. V. *et al.* Beta-blocker use and survival in patients with ventricular fibrillation or symptomatic ventricular tachycardia: the Antiarrhythmics Versus Implantable Defibrillators (AVID) trial. *J. Am. Coll. Cardiol.* **34**, 325–333 (1999).
- Schwartz, P. J. *et al.* Prevention of sudden cardiac death after a first myocardial infarction by pharmacologic or surgical antiadrenergic interventions. *J. Cardiovasc. Electrophysiol.* **3**, 2–16 (1992).
- Thomas, D., Kiehn, J., Katus, H. A. & Karle, C. A. Adrenergic regulation of the rapid component of the cardiac delayed rectifier potassium current, I(Kr), and the underlying hERG ion channel. *Basic Res. Cardiol.* **99**, 279–287 (2004).
- Cutler, M. J., Jeyaraj, D. & Rosenbaum, D. S. Cardiac electrical remodeling in health and disease. *Trends Pharmacol. Sci.* **32**, 174–180 (2011).
- Bers, D. M. Calcium cycling and signaling in cardiac myocytes. *Annu. Rev. Physiol.* **70**, 23–49 (2008).
- Ieda, M. *et al.* Sema3a maintains normal heart rhythm through sympathetic innervation patterning. *Nat. Med.* **13**, 604–612 (2007).
- Lorentz, C. U. *et al.* Heterogeneous ventricular sympathetic innervation, altered β adrenergic receptor expression, and rhythm instability in mice lacking p75 neurotrophin receptor. *Am. J. Physiol. Heart Circ. Physiol.* **298**, H1652–H1660 (2010).
- Li, W., Knowlton, D., Van Winkle, D. M. & Habecker, B. A. Infarction alters both the distribution and noradrenergic properties of cardiac sympathetic neurons. *Am. J. Physiol. Heart Circ. Physiol.* **286**, H2229–H2236 (2004).
- Dae, M. W., O'Connell, J. W., Botvinick, E. H. & Chin, M. C. Acute and chronic effects of transient myocardial ischemia on sympathetic nerve activity, density, and norepinephrine content. *Cardiovasc. Res.* **30**, 270–280 (1995).

15. Simula, S. *et al.* Cardiac adrenergic innervation within the first 3 months after acute myocardial infarction. *Clin. Physiol.* **20**, 366–373 (2000).
16. Stanton, M. S. *et al.* Regional sympathetic denervation after myocardial infarction in humans detected noninvasively using I-123-metaiodobenzylguanidine. *J. Am. Coll. Cardiol.* **14**, 1519–1526 (1989).
17. Barber, M. J., Mueller, T. M., Henry, D. P., Felten, S. Y. & Zipes, D. P. Transmural myocardial infarction in the dog produces sympathectomy in noninfarcted myocardium. *Circulation* **67**, 787–796 (1983).
18. Boogers, M. J. *et al.* Cardiac sympathetic denervation assessed with 123-iodine metaiodobenzylguanidine imaging predicts ventricular arrhythmias in implantable cardioverter-defibrillator patients. *J. Am. Coll. Cardiol.* **55**, 2769–2777 (2010).
19. Nishisato, K. *et al.* Impaired cardiac sympathetic innervation and myocardial perfusion are related to lethal arrhythmia: quantification of cardiac tracers in patients with ICDs. *J. Nucl. Med.* **51**, 1241–1249 (2010).
20. Fallavollita, J. A. *et al.* Regional myocardial sympathetic denervation predicts the risk of sudden cardiac arrest in ischemic cardiomyopathy. *J. Am. Coll. Cardiol.* **63**, 141–149 (2014).
21. Vaseghi, M., Lux, R. L., Mahajan, A. & Shivkumar, K. Sympathetic stimulation increases dispersion of repolarization in humans with myocardial infarction. *Am. J. Physiol. Heart Circ. Physiol.* **302**, H1838–H1846 (2012).
22. Rubart, M. & Zipes, D. P. Mechanisms of sudden cardiac death. *J. Clin. Invest.* **115**, 2305–2315 (2005).
23. Gardner, R. T. & Habecker, B. A. Infarct-derived chondroitin sulfate proteoglycans prevent sympathetic reinnervation after cardiac ischemia-reperfusion injury. *J. Neurosci.* **33**, 7175–7183 (2013).
24. Lorentz, C. U. *et al.* Sympathetic denervation of peri-infarct myocardium requires the p75 neurotrophin receptor. *Exp. Neurol.* **249**, 111–119 (2013).
25. Bai, R. *et al.* Ablation of ventricular arrhythmias in arrhythmogenic right ventricular dysplasia/cardiomyopathy: arrhythmia-free survival after endo-epicardial substrate based mapping and ablation. *Circulation* **4**, 478–485 (2011).
26. Lang, B. *et al.* Systemic modulation of the proteoglycan receptor PTP σ promotes functional recovery after spinal cord injury. *Nature*; doi: 10.1038/nature13974 (2014).
27. Parrish, D. C. *et al.* Infarction-induced cytokines cause local depletion of tyrosine hydroxylase in cardiac sympathetic nerves. *Exp. Physiol.* **95**, 304–314 (2009).
28. Kimura, K. *et al.* Cardiac sympathetic rejuvenation: a link between nerve function and cardiac hypertrophy. *Circ. Res.* **100**, 1755–1764 (2007).
29. Shi, X. & Habecker, B. A. gp130 cytokines stimulate proteasomal degradation of tyrosine hydroxylase via extracellular signal regulated kinases 1 and 2. *J. Neurochem.* **120**, 239–247 (2012).
30. Dobaczewski, M. *et al.* Extracellular matrix remodeling in canine and mouse myocardial infarcts. *Cell Tissue Res.* **324**, 475–488 (2006).
31. Banville, I. & Gray, R. A. Effect of action potential duration and conduction velocity restitution and their spatial dispersion on alternans and the stability of arrhythmias. *J. Cardiovasc. Electrophysiol.* **13**, 1141–1149 (2002).
32. Knollmann, B. C., Schober, T., Petersen, A. O., Sirenko, S. G. & Franz, M. R. Action potential characterization in intact mouse heart: steady-state cycle length dependence and electrical restitution. *Am. J. Physiol. Heart Circ. Physiol.* **292**, H614–H621 (2007).
33. Lue, W. M. & Boyden, P. A. Abnormal electrical properties of myocytes from chronically infarcted canine heart. Alterations in Vmax and the transient outward current. *Circulation* **85**, 1175–1188 (1992).
34. Bru-Mercier, G. *et al.* Expression of heart K⁺ channels in adrenalectomized and catecholamine-depleted reserpine-treated rats. *J. Mol. Cell Cardiol.* **35**, 153–163 (2003).
35. Muller, J. E. *et al.* Circadian variation in the frequency of sudden cardiac death. *Circulation* **75**, 131–138 (1987).
36. Scheer, F. A. *et al.* Impact of the human circadian system, exercise, and their interaction on cardiovascular function. *Proc. Natl Acad. Sci. USA* **107**, 20541–20546 (2010).
37. Wilson, L. D., Wan, X. & Rosenbaum, D. S. Cellular alternans: a mechanism linking calcium cycling proteins to cardiac arrhythmogenesis. *Ann. N. Y. Acad. Sci.* **1080**, 216–234 (2006).
38. Myles, R. C., Wang, L., Kang, C., Bers, D. M. & Ripplinger, C. M. Local beta-adrenergic stimulation overcomes source-sink mismatch to generate focal arrhythmia. *Circ. Res.* **110**, 1454–1464 (2012).
39. Erickson, J. R. *et al.* Diabetic hyperglycaemia activates CaMKII and arrhythmias by O-linked glycosylation. *Nature* **502**, 372–376 (2013).
40. Vaseghi, M. *et al.* Cardiac sympathetic denervation in patients with refractory ventricular arrhythmias or electrical storm: intermediate and long term follow up. *Heart Rhythm* **11**, 6 (2014).
41. Lopez-Sendon, J. *et al.* Expert consensus document on beta-adrenergic receptor blockers. *Eur. Heart J.* **25**, 1341–1362 (2004).
42. Cao, J. M. *et al.* Nerve sprouting and sudden cardiac death. *Circ. Res.* **86**, 816–821 (2000).
43. Cao, J. M. *et al.* Relationship between regional cardiac hyperinnervation and ventricular arrhythmia. *Circulation* **101**, 1960–1969 (2000).
44. Zhou, S. *et al.* Mechanisms of cardiac nerve sprouting after myocardial infarction in dogs. *Circ. Res.* **95**, 76–83 (2004).
45. Hasan, W. *et al.* Sympathetic hyperinnervation and inflammatory cell NGF synthesis following myocardial infarction in rats. *Brain Res.* **1124**, 142–154 (2006).
46. Oh, Y. S. *et al.* Spatial distribution of nerve sprouting after myocardial infarction in mice. *Heart Rhythm* **3**, 728–736 (2006).
47. Moss, A. J. *et al.* Prophylactic implantation of a defibrillator in patients with myocardial infarction and reduced ejection fraction. *N. Engl. J. Med.* **346**, 877–883 (2002).
48. Goldenberg, I. *et al.* Long-term benefit of primary prevention with an implantable cardioverter-defibrillator: An Extended 8-Year Follow-Up Study of the Multicenter Automatic Defibrillator Implantation Trial II. *Circulation* **122**, 1265–1271 (2010).
49. Nerbonne, J. M. Mouse models of arrhythmogenic cardiovascular disease: challenges and opportunities. *Curr. Opin. Pharmacol.* **15**, 107–114 (2014).
50. Jouven, X. *et al.* Heart-rate profile during exercise as a predictor of sudden death. *N. Engl. J. Med.* **352**, 1951–1958 (2005).
51. Elchebly, M. *et al.* Neuroendocrine dysplasia in mice lacking protein tyrosine phosphatase sigma. *Nat. Genet.* **21**, 330–333 (1999).
52. Faggioni, M. *et al.* Accelerated sinus rhythm prevents catecholaminergic polymorphic ventricular tachycardia in mice and in patients. *Circ. Res.* **112**, 689–697 (2013).
53. Nebel, M. *et al.* Nicotinic acid adenine dinucleotide phosphate (NAADP)-mediated calcium signaling and arrhythmias in the heart evoked by β -adrenergic stimulation. *J. Biol. Chem.* **288**, 16017–16030 (2013).
54. Bayly, P. V. *et al.* Estimation of conduction velocity vector fields from epicardial mapping data. *IEEE Trans. Biomed. Eng.* **45**, 563–571 (1998).
55. Verrier, R. L. *et al.* Microvolt T-wave alternans physiological basis, methods of measurement, and clinical utility—consensus guideline by International Society for Holter and Noninvasive Electrocardiology. *J. Am. Coll. Cardiol.* **58**, 1309–1324 (2011).
56. Myles, R. C., Burton, F. L., Cobbe, S. M. & Smith, G. L. Alternans of action potential duration and amplitude in rabbits with left ventricular dysfunction following myocardial infarction. *J. Mol. Cell Cardiol.* **50**, 510–521 (2011).
57. Wang, L. *et al.* Optical mapping of sarcoplasmic reticulum Ca²⁺ in the intact heart: ryanodine receptor refractoriness during alternans and fibrillation. *Circ. Res.* **114**, 1410–1421 (2014).

Acknowledgements

This work was supported by NHLBI HL093056 and HL068231 (B.A.H.) and HL111600 (C.M.R.); NINDS NS25713 (J.S.); the American Heart Association 12SDG9010015 (C.M.R.); and an Oregon Brain Institute Neurobiology of Disease Fellowship (R.T.G.). We thank Dr Michel Tremblay (McGill University, Montreal, Canada) for providing the PTP σ transgenic mice.

Author contributions

R.T.G., L.W., C.M.R. and B.A.H. designed experimental approaches and analysed data. R.T.G. performed all surgical procedures and drug injections. B.T.L., J.C. and J.S. designed and developed the intracellular sigma peptide. R.T.G. and C.L.D. carried out immunohistochemistry, quantified innervation density and infarct size and analysed ECG recordings. W.R.W., C.L.D. and R.T.G. collected tissue and carried out HPLC analysis of NE. L.W., C.M.R. and R.T.G. performed and analysed optical mapping experiments. All authors discussed results and commented on the manuscript. R.T.G. and B.A.H. wrote the manuscript.

Additional information

Supplementary Information accompanies this paper at <http://www.nature.com/naturecommunications>

Competing financial interests: The authors declare no competing financial interests.

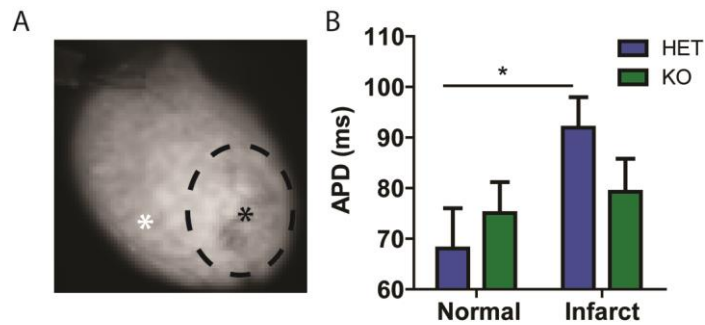
Reprints and permission information is available online at <http://npng.nature.com/reprintsandpermissions/>

How to cite this article: Gardner, R. T. *et al.* Targeting protein tyrosine phosphatase σ after myocardial infarction restores cardiac sympathetic innervation and prevents arrhythmias. *Nat. Commun.* 6:6235 doi: 10.1038/ncomms7235 (2015).

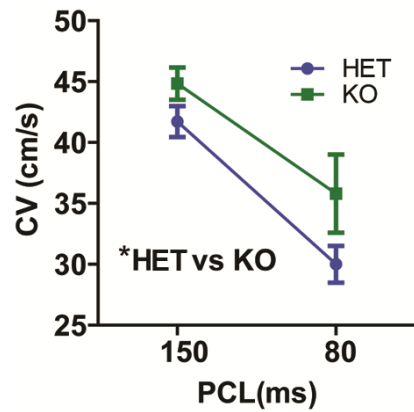


This work is licensed under a Creative Commons Attribution 4.0 International License. The images or other third party material in this article are included in the article's Creative Commons license, unless indicated otherwise in the credit line; if the material is not included under the Creative Commons license, users will need to obtain permission from the license holder to reproduce the material. To view a copy of this license, visit <http://creativecommons.org/licenses/by/4.0/>

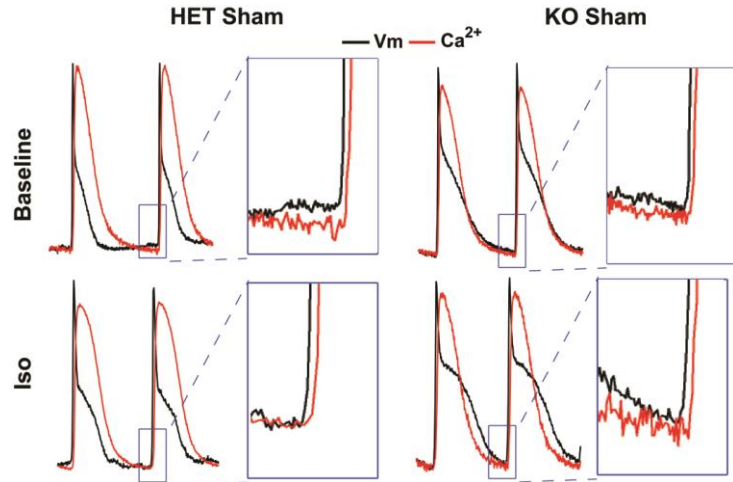
Supplementary Figures



Supplementary Figure 1. Regional variation in APD following MI. (A) An image of a heart prepared for mapping. The dotted area identifies the approximate location of infarcted myocardium. The black asterisk represents the location where APD was measured for the infarct, while the white asterisk identifies where APD was measured for normal, un-injured myocardium. **(B)** Quantification of regional APD. HET hearts have a significantly longer APD within the infarct compared to normal tissue. The reinnervated KO hearts, however, have similar APD in both regions. The regional differences observed in HET hearts explain the greater dispersion of APD (as measured by IQR). Data are mean \pm SEM, $n=5$ hearts/genotype. $*p<.05$ using a two-way ANOVA and Bonferroni post-test.



Supplementary Figure 2. Conduction velocity (CV) following MI. As expected, changing the pacing interval from 150 ms (400 bpm) to 80 ms (750 bpm) results in a rate-dependent slowing of CV in both HET and KO hearts. KO hearts, however, have significantly faster CV overall. Data are mean \pm SEM, n=5 hearts/genotype. * p<.05 using a two-way ANOVA and Bonferroni post-test.



Supplementary Figure 3. Ca^{2+} handling is normal in sham hearts. Representative optical Ca^{2+} transients (Ca_T) in HET and KO sham hearts at baseline, and with isoproterenol (Iso). Note that the Ca_T upstroke follows V_m depolarization even in the presence of Iso. Insets show an expanded time scale of V_m and Ca_T upstrokes.